Title

Subtropical clouds key to Southern Ocean teleconnections to the tropical Pacific

Journal

Proceedings of the National Academy of Sciences of the United States of America, 119(34)

ISSN

0027-8424

Authors

Kim, Hanjun
Kang, Sarah M
Kay, Jennifer E
et al.

Publication Date

2022-08-23

DOI

10.1073/pnas.2200514119

Peer reviewed

PNAS RESEARCH ARTICLE | EARTH, ATMOSPHERIC, AND PLANETARY SCIENCES

Subtropical clouds key to Southern Ocean teleconnections to the tropical Pacific

Hanjun Kim[a], Sarah M. Kang[a,1], Jennifer E. Kay[b,c], and Shang-Ping Xie[d]

Edited by Dennis Hartmann, University of Washington, Seattle, WA; received January 11, 2022; accepted May 26, 2022

Excessive precipitation over the southeastern tropical Pacific is a major common bias that persists through generations of global climate models. While recent studies suggest an overly warm Southern Ocean as the cause, models disagree on the quantitative importance of this remote mechanism in light of ocean circulation feedback. Here, using a multimodel experiment in which the Southern Ocean is radiatively cooled, we show a teleconnection from the Southern Ocean to the tropical Pacific that is mediated by a shortwave subtropical cloud feedback. Cooling the Southern Ocean preferentially cools the southeastern tropical Pacific, thereby shifting the eastern tropical Pacific rainbelt northward with the reduced precipitation bias. Regional cloud locking experiments confirm that the teleconnection efficiency depends on subtropical stratocumulus cloud feedback. This subtropical cloud feedback is too weak in most climate models, suggesting that teleconnections from the Southern Ocean to the tropical Pacific are stronger than widely thought.

double ITCZ bias | subtropical stratocumulus cloud feedback | climate teleconnection

Significance

Global climate models suffer from common errors of excessive precipitation over the southeastern tropical Pacific. This tropical precipitation bias limits the skill of model simulations and the confidence in future climate projections. While the underestimated subtropical low clouds typically are considered the main culprit of the tropical precipitation bias, more recent studies propose the overly warm Southern Ocean as another possible cause, but models disagree on the quantitative importance of this remote contribution. Here, we show the Southern Ocean–driven teleconnection mechanism mediated by subtropical low cloud feedback, which is erroneously weak in climate models. This suggests that the impact of the Southern Ocean bias on the tropical precipitation bias is likely to be stronger than recent studies suggest.

Convective heating in the intertropical convergence zone (ITCZ) drives the global atmospheric circulation, and its change affects climate conditions around the world, as illustrated by El Niño–Southern Oscillation. While the eastern Pacific ITCZ is displaced north of the Equator in observations, it is too symmetric in climate models with a zonal rain band on either side of the Equator (1). This double ITCZ bias was first reported more than a quarter-century ago (2) and stubbornly persists to this day (3), severely limiting the skills in climate predictions and projections (4–8).

Earlier studies of the ITCZ asymmetry focused on tropical ocean–atmosphere interactions (9) and the role of tropical continental geometry in triggering the latitudinal asymmetry (10). Specifically, models were found incapable of simulating the realistic amount and distribution of inversion-capped low clouds off the Pacific coast of South America. Underestimated low clouds cause profound warm sea surface temperature (SST) bias via the positive feedback between the SST and low clouds: An increase in low cloud amount reduces downward solar radiation and cools the local SST while the SST cooling increases the atmospheric stability and hence low cloud amount (11). Prescribing the cloud shortwave radiative cooling effect (12) or strengthening the positive low cloud–SST feedback (10) led to the reduced ITCZ bias. The critical role of low clouds in the basin-scale ITCZ motivated major field experiments in the 2000s (13, 14). The smoothed Andes topography (15–17) and overly weak ocean upwelling off the southeast-slanted South American coast (18, 19) were considered to cause low cloud biases, but the increased model resolution has so far failed to improve consistently the simulation of low cloud deck off South America and hence the ITCZ (20, 21).

The above tropical view of the ITCZ asymmetry has recently given way to a global view based on interhemispheric energetics. The ITCZ displaces into the hemisphere with excessive net energy flux into the atmospheric column in order for the atmospheric meridional energy transport to balance (22). Excessive solar radiation into the Southern Ocean due to cloud biases in the circumpolar storm tracks was suggested to cause a warm bias in the Southern Hemisphere and hence the double ITCZ bias (23, 24). Climate model experiments have been carried out to test this connection between the biases in Southern Ocean cloud radiative effect and the ITCZ but have yielded mixed results. While the Southern Ocean contribution to the double ITCZ bias was confirmed by model experiments without a dynamic ocean (25), fully coupled model experiments tend to show a markedly damped Southern Ocean effect on the tropical Pacific as ocean transport reduces the burden of the atmospheric energy transport (26–29). While recent attention has been directed largely to the ocean circulation damping effect (30, 31), the possibility remains of subtropical low cloud–SST feedback mediating the Southern Ocean effect on the ITCZ bias. An earlier study (32) suggested this possibility based on a comparison of

Author contributions: H.K. and S.M.K. designed research; H.K. performed research; J.E.K. suggested regional cloud locking experiments and provided related resources; S.-P.X. provided remarkable improvement in the manuscript storyline; and H.K., S.M.K., J.E.K., and S.-P.X. wrote the paper.

The authors declare no competing interest.

This article is a PNAS Direct Submission.

[1]To whom correspondence may be addressed. Email: skang@unist.ac.kr.

This article contains supporting information online at http://www.pnas.org/lookup/suppl/doi:10.1073/pnas.2200514119/-/DCSupplemental.

Published August 15, 2022.

two models but did not rule out many other differences between the models that could cause the difference in the ITCZ response.

We report on a set of coordinated multimodel experiments designed to test the hypothesis by applying the same top-of-atmosphere (TOA) radiative forcing over the Southern Ocean to investigate the Southern Ocean–driven teleconnection pattern. We show that Southern Ocean cooling indeed causes a northward displacement of the ITCZ, but the magnitude of the response strongly depends on subtropical low cloud–SST feedback, a result that integrates the work on the ITCZ bias over the past quarter-century in a unified framework. The importance of subtropical low cloud feedback is further corroborated by deliberately turning off the feedback in a model.

The Teleconnection from the Southern Ocean to the Tropical Pacific

As part of the Extratropical–Tropical Interaction Model Intercomparison Project (ETIN-MIP) ensemble (33), eight fully coupled models are perturbed by reducing the solar flux between 65°S and 45°S (denoted as SEXT; *SI Appendix*, Fig. S1). The robust forced signal is obtained as the multimodel mean response after the fast adjustment period (i.e., over years 101–150). The Southern Ocean cooling causes a wedge-like, triangular cooling patch extending from the southeastern Pacific to the zonal band across the equatorial Pacific (Fig. 1*A*, marked by the yellow triangle). As a result, the southeastern tropical Pacific cooling is more pronounced than the northeastern counterpart, leading to a northward shift of the eastern Pacific ITCZ (Fig. 1*B*).

The Southern Ocean–induced teleconnection pattern revealed from ETIN-MIP SEXT simulations is consistent with the tropical Pacific climate pattern congruent with the Southern Ocean radiation biases identified via Climate Model Intercomparison Project (CMIP)-based regression (Fig. 1 *C* and *D*). Specifically, SST and precipitation are regressed onto the shortwave component of TOA cloud radiative effect (SWCRE) over 65°S–45°S via 91 CMIP5/6 historical simulations averaged between 1980 and 2005. The tropical Pacific climate patterns associated with the colder Southern Ocean (Fig. 1 *C* and *D*) largely resemble those of ETIN-MIP SEXT simulations (Fig. 1 *A* and *B*). That is, the models with stronger SWCRE cooling over the Southern Ocean are associated with a stronger triangular cooling patch, an enhanced meridional SST asymmetry over the eastern tropical Pacific (Fig. 1*C*), and a more northward-shifted eastern Pacific ITCZ with reduced precipitation over the southeastern Pacific (Fig. 1*D*). A high degree of similarity between CMIP intermodel regression and ETIN-MIP SEXT simulations suggests a robust teleconnection between the Southern Ocean radiation bias and the tropical Pacific climate pattern.

The question remains as to why ETIN-MIP SEXT simulations exhibit a considerable intermodel spread in the magnitude of tropical climate response, evident from the zonally averaged profiles in Fig. 1 *A* and *B* (also *SI Appendix*, Figs. S2 and S3).

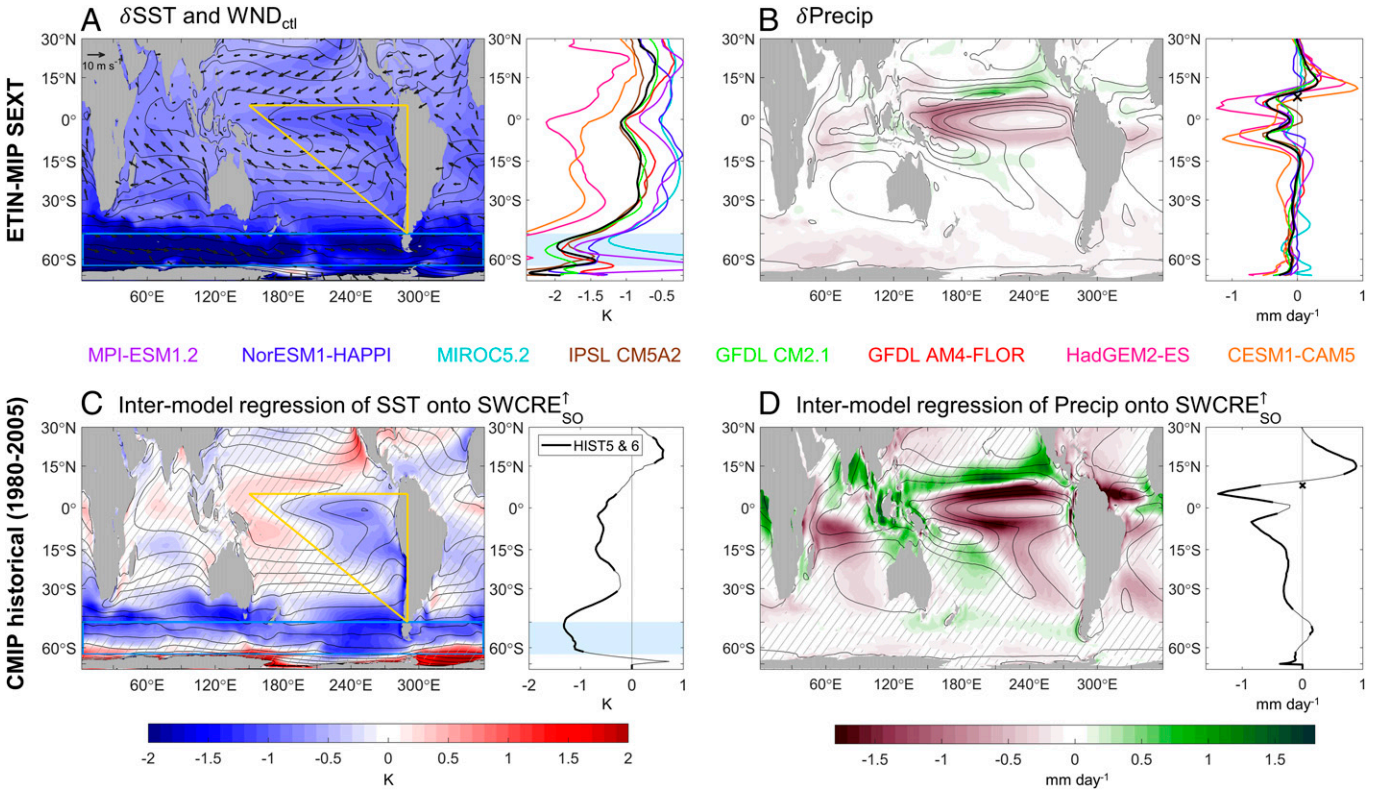

Fig. 1. The impact of Southern Ocean cooling on the tropical Pacific. The multimodel mean responses averaged over years 101–150 in (*A*) SST and (*B*) precipitation for the ETIN-MIP SEXT simulations. In *A*, the multimodel mean climatological surface winds are shown in arrows. The respective right panel shows the eastern Pacific average in each model, with the multimodel mean in black. Intermodel regression of the annual-mean (*C*) SST and (*D*) precipitation onto the upward SWCRE over 65°S–45°S ($SWCRE^{\uparrow}_{SO}$) using historical simulations of 39 CMIP5 and 52 CMIP6 models averaged between 1980 and 2005 (*SI Appendix*, Table S1 for model list). The regression coefficients are multiplied by two intermodel SDs of $SWCRE_{SO}$, comparable to the forcing amplitude of ETIN-MIP SEXT (*SI Appendix*, Fig. S1), to ease comparison with the ETIN-MIP results. The respective right panel shows the eastern Pacific (230°E–300°E) average. The region with the regression coefficients statistically different from zero is unhatched in the maps and denoted as thicker lines for the eastern Pacific average, determined via two-sided Student *t* test with 95% confidence interval. In *A* and *C*, the forcing region between 65°S and 45°S is indicated by blue rectangles, and the triangular cooling patch is marked by yellow triangles. In *B* and *D*, the multimodel mean position of the climatological eastern Pacific ITCZ, defined by the precipitation maximum, is denoted with a cross symbol. The contours in maps indicate the corresponding multimodel mean climatology.

This intermodel spread indicates the model dependence of the efficiency in the Southern Ocean radiative impact on tropical Pacific climate. To understand what controls the strength of the Southern Ocean–tropics teleconnection, we explore the mechanisms for the connection.

Mechanisms for the Teleconnection

We investigate the mechanisms of Southern Ocean–driven equatorward teleconnection via ETIN-MIP SEXT simulations (Fig. 2). To study the initial evolution of the triangular cooling patch over the South Pacific, we carried out a 22-member ensemble SEXT simulation for the first 5 y (*SI Appendix*, Fig. S4 and *Materials and Methods*).

With the reduced solar flux over the Southern Ocean, the colder and drier air at high latitudes is diffused by atmospheric eddies and then advected equatorward by near-surface southeasterlies along the west coast of South America (34, 35). We consider this advection of cold anomalies by the climatological winds as the leading-order teleconnection mechanism. Indeed, the South Pacific cooling pattern closely follows the climatological surface wind pattern, in the long-term mean (Fig. 1*A* and *SI Appendix*, Fig. S2) as well as in the initial period (*SI Appendix*, Fig. S4*A*). The quasi-equilibrated SST response pattern is established within the first 3 y after the imposed Southern Ocean cooling (*SI Appendix*, Fig. S4*A*), suggesting the importance of ocean mixed layer processes.

Along the equatorward teleconnection pathway from the Southern Ocean to the tropics, the cold anomalies are amplified in the eastern Pacific basin by three mechanisms: wind-evaporation–SST (WES) feedback (36), coastal upwelling, and subtropical stratocumulus cloud feedback (32). In response to the Southern Ocean cooling, the extratropical jet intensifies, and thus the anomalous anticyclonic circulation develops on the equatorward side of the climatological jet position (Fig. 2*A* and *SI Appendix*, Fig. S4*C*). The resulting anomalous southerlies increase evaporative cooling, facilitating the equatorward propagation of cold anomalies into the subtropics (37). As subtropical cold anomalies are preferentially advected along the eastern basin (Fig. 1*A*), the subtropical anticyclonic system is intensified to the east (Fig. 2 *A* and *B*). This leads to wind-induced sea surface evaporation and amplified cooling over the southeastern tropical Pacific (25, 38). Indeed, cold anomalies coincide with enhanced evaporation due to wind speed changes (LH_{wnd}; Figs. 1*A* and 2*B*) from the initial stage (*SI Appendix*, Fig. S4 *A* and *D*). This WES feedback thus promotes the southeastern tropical Pacific cooling set by climatological advection. The southeastern Pacific cooling is further amplified as intensified southeasterly winds strengthen oceanic upwelling along the west coast of South America. The stronger coastal upwelling can be inferred from downward surface energy flux response, indicative of increased heat taken up by the ocean (*SI Appendix*, Fig. S4*F*).

The southeastern Pacific cooling is additionally amplified by the stratocumulus cloud feedback off the west coast of subtropical continents (11, 39) (Fig. 2 *C* and *D* and *SI Appendix*, Fig. S4*E*). We estimate this SST–stratocumulus feedback by regressing the deseasonalized and detrended monthly anomalies in TOA SWCRE onto local SST anomalies (*Materials and Methods*). The regression coefficients are positive over the west coast of major continents in the models participating in ETIN-MIP as well as in observations (Fig. 2*C* and *SI Appendix*, Fig. S5), indicative of the positive feedback between the subtropical stratocumulus and underlying SST.

When the Southern Ocean cooling effect reaches the equatorial Pacific through the eastern basin, equatorial cooling is

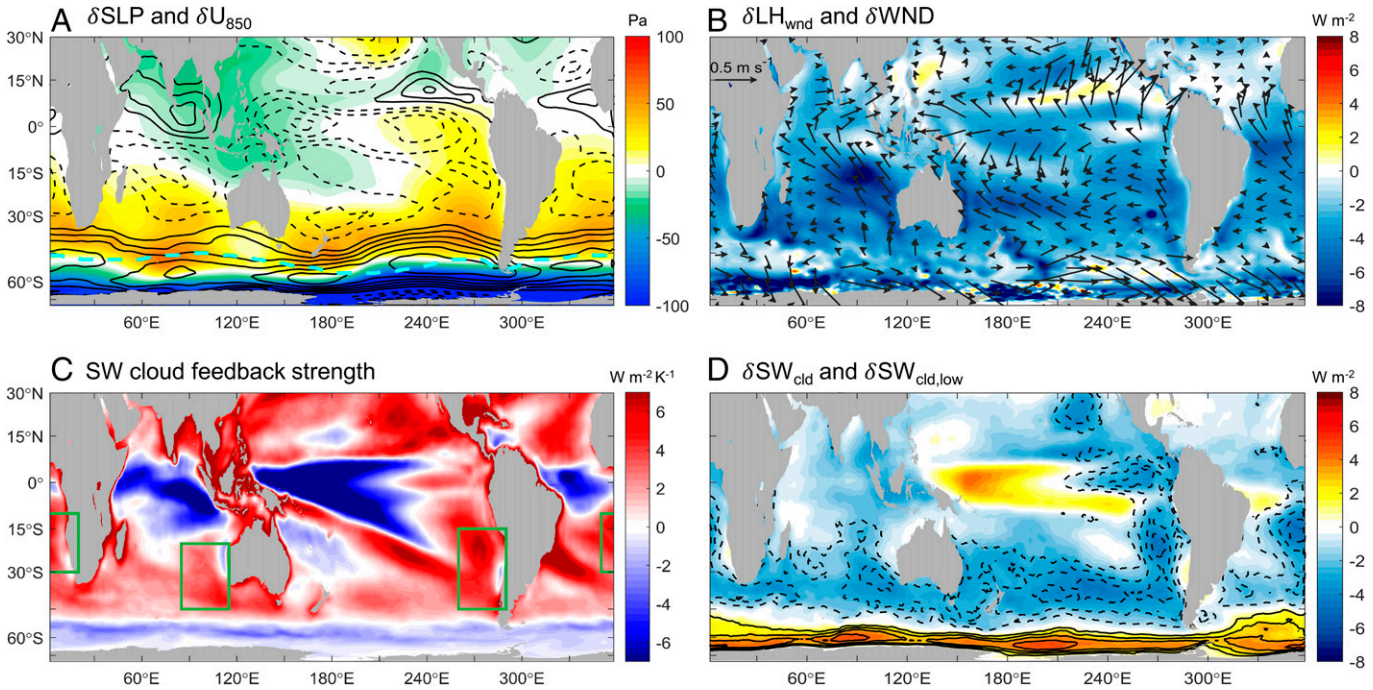

Fig. 2. The Southern Ocean–tropics teleconnection mechanism in ETIN-MIP SEXT. (*A*) The sea level pressure responses and the zonal wind responses at 850 hPa (westerly anomalies in solid and easterly anomalies in dashed contours; 0.1 m/s interval), with a dashed cyan line denoting the climatological jet, calculated as the position of 850 hPa zonal wind maximum. (*B*) The downward positive latent heat flux response due to surface wind speed changes (*Materials and Methods*) and the surface wind response (arrows). (*C*) The shortwave cloud feedback strength in the reference climate (CF; *Materials and Methods*). Green boxes indicate the regions used to define CF averaged over major Southern Hemisphere continents (CF_{wSH}). (*D*) The surface SW cloud radiative anomalies (*Materials and Methods*) and that due to low cloud changes (downward in solid and upward in dashed contours; 1 W/m interval; *Materials and Methods*). All variables are for the multimodel mean averaged over years 101–150.

intensified by Bjerknes feedback: An initial increase in zonal SST gradient strengthens the equatorial easterlies, which lift the thermocline and increase the upwelling of subsurface water in the east, thereby providing additional cooling. The enhanced easterlies also lead to evaporative cooling along the Equator (Fig. 2*B* and *SI Appendix*, Fig. S4*D*), further contributing to strengthening the Pacific cold tongue. In sum, Southern Ocean cooling induces a triangular cold patch over the South Pacific (Fig. 1 *A* and *C*) via the abovementioned atmospheric and oceanic feedbacks, reminiscent of the South Pacific meridional mode (40) in the context of coupled internal variability.

Intermodel Diversity and the Subtropical Stratocumulus Cloud Feedback

Among ETIN-MIP models, a stronger cooling patch over the South Pacific is associated with an enhanced north-minus-south SST anomaly in the eastern Pacific (*SI Appendix*, Fig. S6*A*) and a more northward shift in the eastern Pacific ITCZ, corresponding to a reduced double-ITCZ bias (*SI Appendix*, Fig. S6*B*). We now explain the intermodel diversity in the triangular cooling by examining the intermodel differences in the amplifying mechanisms along the eastern Pacific teleconnection pathway discussed in the previous section.

To assess the relative contributions of individual amplifying mechanisms to the intermodel difference in the triangular cooling amplitude, we regress the components of surface flux responses onto the SST response in the eastern Pacific basin (230°E–300°E; *SI Appendix*, Fig. S7). The regression analysis indicates that intermodel diversity in the eastern Pacific cooling arises primarily from differences in the shortwave cloud radiative anomalies. Indeed, the models with a stronger stratocumulus cloud feedback along the subtropical west coast of South America (CF_{wSA}; area-averaged CF within the green box in Fig. 3*A*) tend to show a larger triangular cooling (Fig. 3 *A* and *B*). The stronger southeastern subtropical cooling then intensifies the mean southeasterlies (Fig. 3*A*) and enhances evaporative cooling on the equatorward side (*SI Appendix*, Fig. S7), thereby producing the stronger triangular cooling patch. As a consequence, CF_{wSA} modulates the extent of the eastern Pacific ITCZ shift, as can be seen from their strong correlation at 0.89 (Fig. 3*C*). Note that CF_{wSA} also regulates the strength of global-mean surface cooling (*SI Appendix*, Fig. S8), consistent with previous studies on global climate sensitivity (41, 42).

We demonstrate the influence of subtropical stratocumulus clouds by repeating the SEXT simulation in the Community Earth System Model version 1 and Community Atmosphere Model version 5 (CESM1-CAM5) but with cloud radiative feedbacks regionally disabled off the west coast of South America (*Materials and Methods*). The difference from the interactive cloud simulations quantifies the effect of cloud radiative feedback (Fig. 4). In the regional cloud locked simulation, the cooling induced by the shortwave cloud effect is removed over a narrow region in the southeastern Pacific (Fig. 4*B*), and the cooling response is substantially damped throughout the tropical Pacific (Fig. 4 *D*–*F*). A damped southeastern Pacific cooling acts to reduce anomalous easterlies, weakening both the WES feedback and coastal upwelling. This tight coupling between radiation, atmospheric circulation, and ocean dynamics forms the triangular cooling patch overlapping the enhanced easterlies (Fig. 4*F*). The triangular cooling patch in the southeastern Pacific weakens by 24.7% when stratocumulus cloud feedbacks are locked west of South America (Fig. 3*B*). Locking stratocumulus cloud feedbacks west of all major continents in the

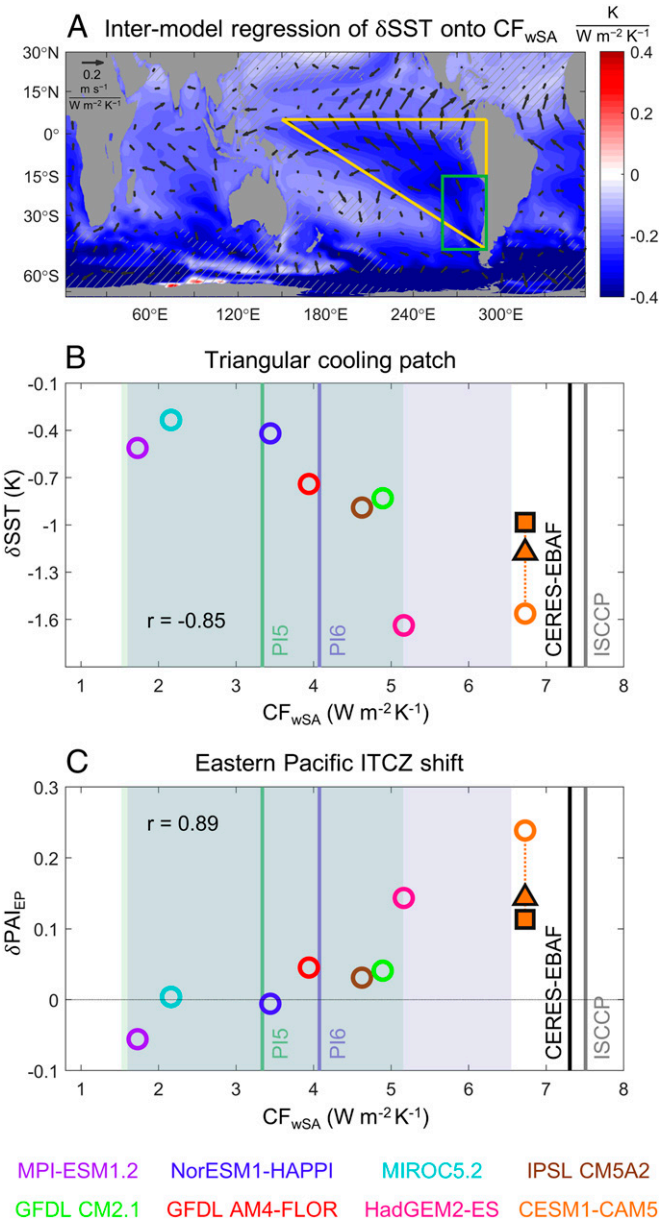

Fig. 3. Attribution of the intermodel diversity to varying estimates of subtropical stratocumulus cloud feedback strength in ETIN-MIP SEXT. (*A*) Intermodel regression of the SST responses (shading) and surface wind responses (arrows) onto the CF_{wSA} (*Materials and Methods*). Green box indicates the region used to define CF_{wSA}. Relationship between CF_{wSA} and (*B*) strength of triangular cooling patch (SST responses within the yellow triangle in *A*) and (*C*) δPAI_{EP}, the precipitation asymmetry index in the eastern Pacific (*Materials and Methods*). The individual models are color coded as in Fig. 1. In *B* and *C*, the Pearson correlation coefficients are inserted. The filled triangle (rectangle) orange symbols indicate the CESM experiment in which clouds are locked west of South America (all major Southern Hemisphere continents). Green (blue) shading indicates ±1 intermodel SD of CF_{wSA} for the 39 CMIP5 (52 CMIP6) models, with the vertical lines in a corresponding color denoting the multimodel mean. The observed estimates of CF_{wSA} are indicated by achromatic vertical lines (*Materials and Methods*).

Southern Hemisphere (indicated by green boxes in Fig. 2*C*) results in a further weakening of the southeastern Pacific cooling by 37.1% relative to the interactive cloud simulations (Fig. 3*B*). Accordingly, the eastern tropical Pacific SST response features an enhanced meridional asymmetry (Fig. 4*F*), with an amplified northward shift of the eastern Pacific ITCZ (Fig. 4*I*). The subtropical stratocumulus cloud feedback west of South America (Southern Hemisphere continents) is responsible for 39.9% (52.5%) of the eastern Pacific ITCZ shifts (Fig. 3*C*).

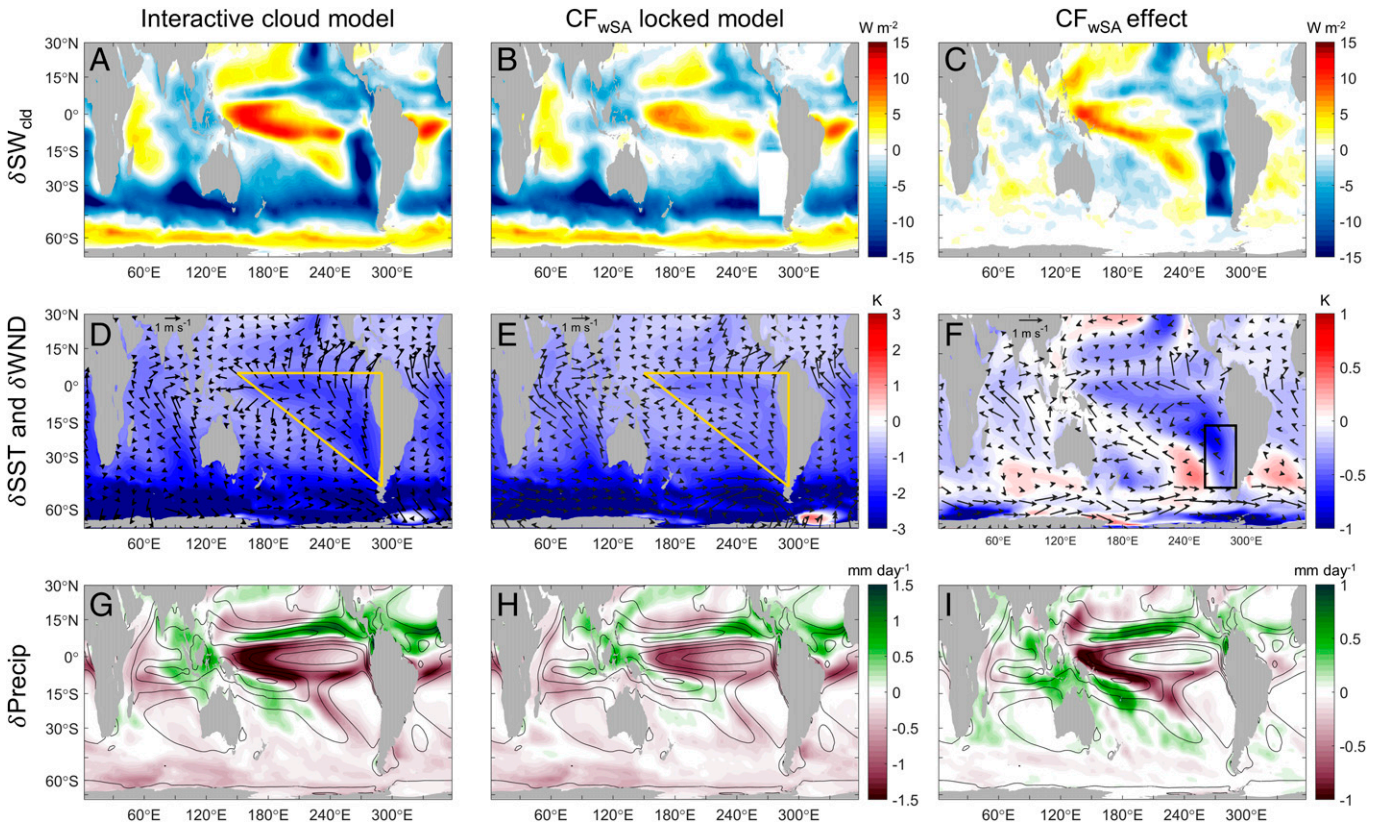

Fig. 4. Comparison of interactive and regional cloud locked CESM1-CAM5 simulations. The response to ETIN-MIP SEXT forcing of (*A*) shortwave cloud radiative anomalies at the surface, (*D*) SST (shadings) and surface wind (arrows), and (*G*) precipitation (shadings) for interactive cloud simulations. (*B*, *E*, *H*) Similar to (*A*, *D*, *G*) but for the simulations with locked clouds west of South America. (*C*, *F*, *I*) The difference between (*A*, *D*, *G*) and (*B*, *E*, *H*), respectively, to quantify the contribution of the amplifying effect of CF_{wSA}. The contours in (*G*, *H*, *I*) indicate the precipitation climatology (2 mm/day interval).

Our regional cloud locking experiments clearly demonstrate that the subtropical stratocumulus cloud feedback is essential for the Southern Ocean–driven teleconnection pattern to be amplified in the tropics. The subtropical stratocumulus cloud feedback is also tightly linked to the zonal-mean ITCZ shift (*SI Appendix*, Fig. S9).

The large intermodel spread of CF_{wSA} prompts us to evaluate the low cloud feedback against observations. All ETIN-MIP models underestimate the strength of stratocumulus cloud feedback west of all major continents (Fig. 3 *B* and *C*). The same is true for most CMIP5/6 models (43) (*SI Appendix*, Fig. S10). This suggests that the Southern Ocean cooling impact on the tropical Pacific is underestimated in the majority of the state-of-the-art climate models (Fig. 3 *B* and *C*). The observed estimate of CF_{wSA} suggests that the Southern Ocean cooling by 0.8PW would cause the eastern Pacific ITCZ shift of $\delta PAI_{EP} = 0.26$, which is comparable to the intermodel SD of eastern Pacific ITCZ location across the ETIN-MIP models (*SI Appendix*, Fig. S11). That is, the Southern Ocean warm bias is likely to be responsible for the tropical Pacific errors if models simulate the subtropical stratocumulus cloud feedback as strongly as in observations.

Discussion

In summary, we have shown that the Southern Ocean cooling shifts the Pacific ITCZ northward by inducing a wedge-like, triangular cooling patch. The teleconnection mechanism is summarized in Fig. 5. The Southern Ocean–tropics teleconnection is initiated by the cold advection following the climatological southeasterlies along the west coast of South America, which is further amplified by the WES effect, coastal upwelling, and positive stratocumulus cloud feedback. In particular, we find that the subtropical stratocumulus CF_{wSA} is the key conduit that controls the strength of the teleconnection. To the extent that CF_{wSA} is substantially underestimated in most state-of-the-art models, the double ITCZ bias could be more related to Southern Ocean cloud biases than recent studies suggest (26–29).

While we discussed the Southern Ocean teleconnection to the tropical Pacific in the context of model bias, it has important implications for future climate projections. For example, the pronounced warming over the Southern Hemisphere high latitude in global warming scenarios, resulting from Antarctic sea-ice loss or reduced Southern Ocean heat uptake, would induce a teleconnection pattern similar to that in SEXT simulations with a reversed sign (44–46). Our results suggest that the strength of this forced teleconnection depends on the subtropical stratocumulus cloud feedback. Importantly, the stratocumulus cloud feedback off the subtropical west coasts of all major continents is substantially underestimated in CMIP5/6 models (*SI Appendix*, Fig. S10), implying that the Southern Ocean effect on the tropical climate is underrepresented in model projections. Our results point to the need for an improved representation of subtropical stratocumulus cloud feedback for realistic simulation of the impact of high-latitude climate change on the tropics. In light of the tropical SST pattern effect, this is ultimately important for constraining climate sensitivity (47–49).

Materials and Methods

Decomposition of the Shortwave Flux Response. The TOA net shortwave flux (SW) responses are decomposed via the Approximate Partial Radiative Perturbation (APRP) method (50):

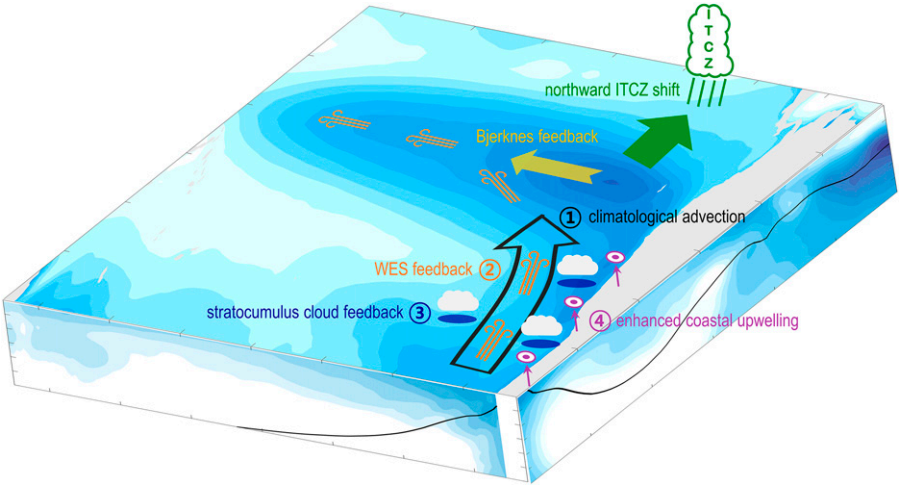

Fig. 5. Schematic of Southern Ocean–tropics teleconnection mechanism. The Southern Ocean cooling propagated into the subtropics by the atmospheric eddies and oceanic Ekman transport is (1) further advected equatorward by the climatological southeasterlies (black arrow) west of South America. The southeastern Pacific cooling is amplified by the interactions between (2) WES feedback, (3) subtropical stratocumulus cloud feedback, and (4) coastal upwelling. The eastern equatorial Pacific cooling is further intensified via Bjerknes feedback. As a consequence, the triangular cooling patch extending from the southeastern Pacific to the zonal band across the equatorial Pacific is manifested by the Southern Ocean–driven teleconnection, inducing the northward shift of the eastern Pacific ITCZ.

$$\delta SW = \delta SW_S + \delta SW_{cld} + \delta SW_{alb} + \delta SW_{ncld}, \quad [1]$$

where the subscripts S, cld, alb, and ncld denote the changes in insolation, cloud, surface albedo, and noncloud atmospheric constituents, with δ indicating the response to perturbations. The δSW at the surface can be similarly decomposed via the APRP method that was recently extended to the surface (51). We confirm that the sum of each component successfully reproduces the actual net SW changes in models, consistent with previous studies (52–55). The TOA δSW_S defines the forcing term in ETIN-MIP simulations (purple in *SI Appendix*, Fig. S1). The δSW_{cld} is referred to as the shortwave cloud radiative anomalies, which differ from the SWCRE, the difference between the total-sky and the clear-sky SW fluxes. Note that both definitions generally yield similar results except in the polar and land regions with high background surface albedo. The δSW_{cld} is further decomposed into the contribution from low cloud changes ($\delta SW_{cld,low}$) by assuming that the cloud radiative anomalies are dominated by low clouds when the absolute ratio of the longwave to shortwave cloud radiative anomalies is less than 0.41 (tan22.5°) (56). The longwave cloud radiative anomalies are calculated as the annual-mean difference between the all-sky and clear-sky outgoing longwave radiation response.

Subtropical Stratocumulus Cloud Feedback Strength. To estimate the shortwave cloud feedback, the SST and SWCRE at TOA are first interpolated on a 1° × 1° latitude–longitude common grid and then deseasonalized and detrended. We define the shortwave cloud feedback as the SWCRE regressed onto the underlying SSTs at each grid point (*SI Appendix*, Fig. S5). The monthly data from the last 100 y of preindustrial control simulations are used for 39 CMIP5 and 52 CMIP6 models (*SI Appendix*, Table S1). The ETIN-MIP provides the monthly data only in the first and the last 20 y; hence, all available monthly data in the control and SEXT simulations (80 y in total) are used for eight ETIN-MIP models. The SWCRE is used instead of SW_{cld} because the APRP method can be applied to only a subset of CMIP models, for which we confirm that SWCRE and SW_{cld} yield similar regression coefficients with a nearly perfect intermodel correlation (1.00). The CF represents the stratocumulus cloud feedback in the stratocumulus-dominated region off the west coast of subtropical continents (black boxes in *SI Appendix*, Fig. S5) (43, 57). We compute the subtropical stratocumulus cloud feedback by averaging cloud feedback over four regions: west of South America (CF_{wSA}), west of the major Southern Hemisphere continents (CF_{wSH}), west of North America (CF_{wNA}), and west of the major Northern Hemisphere continents (CF_{wNH}). Over these four regions, we additionally calculate the low cloud feedback by regressing monthly SWCRE due to the low cloud (56) onto the underlying SST and compare it with the original cloud feedback calculated with SWCRE deviations (*SI Appendix*, Fig. S12). The low cloud feedback dominates the intermodel spread of cloud feedback, which indicates that cloud feedback in these four regions can indeed be the proxy of stratocumulus cloud feedback. The cloud feedback over these regions is similar in amplitude in all models (*SI Appendix*, Fig. S10), as these major low cloud regimes are governed by the same parameterized processes. It is also worthwhile to note that the cloud feedback is resolution-dependent. For example, CESM1-CAM5 at 1° horizontal resolution exhibits 53.68% damped CF_{wSA} compared to the one at 2° horizontal resolution. This may explain why CESM1-CAM5 at 1° horizontal resolution shows little influence of Southern Ocean shortwave radiation on tropical precipitation (27), while the same model at 2° horizontal resolution exhibits the strongest teleconnection among ETIN-MIP (Fig. 3 *B* and *C*). We further obtain the observed cloud feedback estimate by using the monthly TOA SWCRE from the Clouds and Earth's Radiant Energy Systems Energy Balanced and Filled data version 4.1 (58) and the monthly SST from the Optimum Interpolation Sea Surface Temperature data version 2 (59) from March 2000 to February 2020. Another observed estimate is obtained from the TOA SWCRE monthly data from the International Satellite Cloud Climatology Project H-series products (60) and the monthly Optimum Interpolation Sea Surface Temperature data from January 1984 to December 2016. Note that our observed estimate could be biased due to decadal trends in tropical Pacific SST pattern (49); however, a more refined method of cloud feedback estimation also consistently points to underestimated stratocumulus cloud feedback in CMIP5/6 models (43).

Decomposition of the Latent Heat Flux Response. Using the bulk formula assuming a saturated surface over the ocean, the latent heat flux response (δLH) can be decomposed into the components due to the surface wind speed changes (δLH_{WND}), relative humidity changes at model reference level (δLH_{RH}), near-surface atmospheric stability changes ($\delta LH_{\Delta T}$), and surface temperature changes (δLH_{T_s}) (61):

$$\delta LH = \left(\frac{\overline{LH}}{\overline{WND}}\right)\delta WND + \left(\frac{-\overline{LH}}{e^{-\beta\overline{\Delta T}} - \overline{RH}}\right)\delta RH + \left(\frac{-\beta\overline{LH}\cdot\overline{RH}}{e^{-\beta\overline{\Delta T}} - \overline{RH}}\right)\delta(\Delta T) + (\beta\overline{LH})\delta T_s = \delta LH_{wnd} + \delta LH_{rh} + \delta LH_{tdiff} + \delta LH_{T_s}, \quad [2]$$

where the overbar indicates the reference climatology, WND the surface wind speed, RH the relative humidity at model reference level, $\Delta T = T_{ref} - T_S$, with T_{ref} the reference level temperature and T_S the surface temperature, and $\beta \equiv \frac{L_v}{R_v T_s^2}$ with the latent heat of vaporization $L_v = 2.5 \times 10^6$ J/kg and $R_v = 461.5$ J/kg/K. Note that δLH_{wnd} is calculated as the residual term because of data availability issues with the surface wind speed. We confirm via CESM1-CAM5 data that this indirect estimation of δLH_{wnd} and the direct calculation using surface wind speed output are similar in their pattern and magnitude (*SI Appendix*, Fig. S13).

Precipitation Asymmetry Index. We quantify the eastern Pacific ITCZ shift by calculating the precipitation in the northern tropical eastern Pacific (230°E–290°E, 0°–20°N) minus the precipitation in the southern tropical eastern Pacific (230°E–290°E, 20°S–0°), normalized by the tropical eastern Pacific precipitation (230°E–290°E, 20°S–20°N). This is defined as the precipitation asymmetry index over the tropical eastern Pacific, denoted as PAI_{EP}. A positive PAI_{EP} response indicates a northward eastern Pacific ITCZ shift.

CESM1-CAM5 Ensemble Experiments. To examine the initial adjustment period, we conduct a 22-member ensemble of ETIN-MIP SEXT experiments (33) with CESM1-CAM5 at 2° horizontal resolution (62). Note that CESM1-CAM5 exhibits the strongest teleconnection from the Southern Ocean to the tropics among the models participating in ETIN-MIP (Fig. 3 *B* and *C*). The ensemble members are integrated for 5 y after an abrupt reduction of insolation between 45°S and 65°S on 1 January of subsequent 22 y of a fully spun-up preindustrial control simulation (i.e., 350-y additionally integrated "B_1850_CAM5" component set). We obtain the ensemble-mean climate response by first calculating the difference in each year between the perturbed and control simulations, which are initiated from the same dates, and then taking the average over all ensemble members.

CESM1-CAM5 Regional Cloud Locking Experiments. To evaluate the effect of subtropical stratocumulus cloud feedback on the teleconnection pattern, we conduct regional cloud locking experiments with CESM1-CAM5 (63, 64). The eight cloud parameters are first extracted every 2 h from a randomly chosen 1-year integration of a fully spun-up preindustrial control simulation. In the cloud locking experiments, these cloud parameters are prescribed repeatedly every year in the radiative transfer code. The clouds are locked regionally, either to the west of South America (260°E–290°E and 45°S–15°S) or to the west of all major Southern Hemisphere continents (*SI Appendix*, Fig. S5). Both the SEXT and the control simulations are integrated, with the clouds locked regionally for 150 y. The average response in the last 50 y is used for the analysis. Contrasting the fully interactive and regionally locked cloud simulations elucidates the role of the subtropical stratocumulus cloud feedback on the Southern Ocean–driven teleconnection.

Data, Materials, and Software Availability. Data for ETIN-MIP (65), regional cloud locking and ensemble experiments (66) have been deposited in a publicly accessible database (doi: 10.5281/zenodo.3362615 and 10.5281/zenodo.5792715).

ACKNOWLEDGMENTS. This work has been supported by the National Research Foundation of Korea (Grant NRF-2020R1A2C210150311), funded by the Ministry of Science and ICT of South Korea. H.K. and S.M.K. is supported by the grant from Korea Meteorological Institute. J.E.K. was supported by NSF Grant 1554659 and S.-P.X. by NSF Grant 1934392. All CMIP data are acquired from the Earth System Grid Federation node hosted by Lawrence Livermore National Laboratory, via the Synda Transfer Module (https://prodiguer.github.io/synda/index.html). Computing and data storage resources for the regional cloud locking experiments were provided by the NSF through the Computational and Information Systems Laboratory at the National Center for Atmospheric Research, including the Cheyenne supercomputer (doi:10.5065/D6RX99HX). We express special thanks to all the modeling groups who make CMIP and ETIN-MIP data available and Sungduk Yu for providing the initial conditions and codes for the CESM1-CAM5 experiments. We are also thankful to Hung-Yi Tseng and Yen-Ting Hwang, who generously shared the 13 members of the CESM1-CAM5 ensemble experiment. Lastly, we are deeply grateful to Masahiro Watanabe, Tomo Ogura, Yechul Shin, and Doyeon Kim for helpful discussions on early stage of the work.

Author affiliations: [a]Department of Urban and Environmental Engineering, Ulsan National Institute of Science and Technology, Ulsan 44919, Republic of Korea; [b]Department of Atmospheric and Oceanic Sciences, University of Colorado Boulder, Boulder, CO 80309; [c]Cooperative Institute for Research in Environmental Sciences, Department of Atmospheric and Oceanic Sciences, University of Colorado Boulder, Boulder, CO 80309; and [d]Scripps Institution of Oceanography, University of California San Diego, La Jolla, CA 92093-0206

1. J.-L. Lin, The double-ITCZ problem in IPCC AR4 coupled GCMs: Ocean–atmosphere feedback analysis. *J. Clim.* **20**, 4497–4525 (2007).
2. C. R. Mechoso *et al.*, The seasonal cycle over the tropical Pacific in coupled ocean–atmosphere general circulation models. *Mon. Weather Rev.* **123**, 2825–2838 (1995).
3. B. Tian, X. Dong, The double-ITCZ bias in CMIP3, CMIP5, and CMIP6 models based on annual mean precipitation. *Geophys. Res. Lett.* **47**, e2020GL087232 (2020).
4. Y.-G. Ham, J.-S. Kug, Effects of Pacific Intertropical Convergence Zone precipitation bias on ENSO phase transition. *Environ. Res. Lett.* **9**, 064008 (2014).
5. J.-Y. Lee *et al.*, How are seasonal prediction skills related to models' performance on mean state and annual cycle? *Clim. Dyn.* **35**, 267–283 (2010).
6. R. Seager *et al.*, Strengthening tropical Pacific zonal sea surface temperature gradient consistent with rising greenhouse gases. *Nat. Clim. Chang.* **9**, 517–522 (2019).
7. B. Tian, Spread of model climate sensitivity linked to double-Intertropical Convergence Zone bias. *Geophys. Res. Lett.* **42**, 4133–4141 (2015).
8. Z.-Q. Zhou, S.-P. Xie, Effects of climatological model biases on the projection of tropical climate change. *J. Clim.* **28**, 9909–9917 (2015).
9. S.-P. Xie, "The shape of continents, air-sea interaction, and the rising branch of the hadley circulation" in *The Hadley Circulation: Present, Past and Future, Advances in Global Change Research*, H. F. Diaz, R. S. Bradley, Eds. (Springer, Dordrecht, 2004).
10. S. G. H. Philander *et al.*, Why the ITCZ is mostly north of the Equator. *J. Clim.* **9**, 2958–2972 (1996).
11. S. A. Klein, D. L. Hartmann, The seasonal cycle of low stratiform clouds. *J. Clim.* **6**, 1587–1606 (1993).
12. C.-C. Ma, C. R. Mechoso, A. W. Robertson, A. Arakawa, Peruvian stratus clouds and the tropical Pacific circulation: A coupled ocean-atmosphere GCM study. *J. Clim.* **9**, 1635–1645 (1996).
13. D. J. Raymond *et al.*, EPIC2001 and the coupled ocean–atmosphere system of the tropical east Pacific. *Bull. Am. Meteorol. Soc.* **85**, 1341–1354 (2004).
14. R. Wood *et al.*, The VAMOS Ocean-Cloud-Atmosphere-Land Study Regional Experiment (VOCALS-REx): Goals, platforms, and field operations. *Atmos. Chem. Phys.* **11**, 627–654 (2011).
15. R. Feng, C. J. Poulsen, Andean elevation control on tropical Pacific climate and ENSO: Andean uplift and tropical climate. *Paleoceanography* **29**, 795–809 (2014).
16. K. Takahashi, D. S. Battisti, Processes controlling the mean tropical pacific precipitation pattern. Part I: The Andes and the eastern Pacific ITCZ. *J. Clim.* **20**, 3434–3451 (2007).
17. W. Xu, J.-E. Lee, The Andes and the Southeast Pacific cold tongue simulation. *J. Clim.* **34**, 415–425 (2021).
18. I. Richter, Climate model biases in the eastern tropical oceans: Causes, impacts and ways forward. *Wiley Interdiscip. Rev. Clim. Change* **6**, 345–358 (2015).
19. P. Zuidema *et al.*, Challenges and prospects for reducing coupled climate model SST biases in the Eastern Tropical Atlantic and Pacific Oceans: The U.S. CLIVAR Eastern Tropical Oceans Synthesis Working Group. *Bull. Am. Meteorol. Soc.* **97**, 2305–2328 (2016).
20. Y. Jia, K. J. Richards, H. Annamalai, The impact of vertical resolution in reducing biases in sea surface temperature in a Tropical Pacific Ocean model. *Ocean Model.* **157**, 101722 (2021).
21. R. J. Small *et al.*, A new synoptic scale resolving global climate simulation using the Community Earth System Model. *J. Adv. Model. Earth Syst.* **6**, 1065–1094 (2014).
22. S. M. Kang, Extratropical influence on the tropical rainfall distribution. *Curr. Clim. Change Rep.* **6**, 24–36 (2020).
23. Y.-T. Hwang, D. M. W. Frierson, Link between the double-Intertropical Convergence Zone problem and cloud biases over the Southern Ocean. *Proc. Natl. Acad. Sci. U.S.A.* **110**, 4935–4940 (2013).
24. G. Li, S.-P. Xie, Tropical biases in CMIP5 multimodel ensemble: The excessive equatorial Pacific cold tongue and double ITCZ problems. *J. Clim.* **27**, 1765–1780 (2014).
25. Y.-T. Hwang, S.-P. Xie, C. Deser, S. M. Kang, Connecting tropical climate change with Southern Ocean heat uptake: Tropical climate change and SO heat uptake. *Geophys. Res. Lett.* **44**, 9449–9457 (2017).
26. M. Hawcroft *et al.*, Southern Ocean albedo, inter-hemispheric energy transports and the double ITCZ: Global impacts of biases in a coupled model. *Clim. Dyn.* **48**, 2279–2295 (2017).
27. J. E. Kay *et al.*, Global climate impacts of fixing the southern ocean shortwave radiation bias in the Community Earth System Model (CESM). *J. Clim.* **29**, 4617–4636 (2016).
28. B. Xiang, M. Zhao, Y. Ming, W. Yu, S. M. Kang, Contrasting impacts of radiative forcing in the Southern Ocean versus southern tropics on ITCZ position and energy transport in one GFDL climate model. *J. Clim.* **31**, 5609–5628 (2018).
29. S. Yu, M. S. Pritchard, A strong role for the AMOC in partitioning global energy transport and shifting ITCZ position in response to latitudinally discrete solar forcing in CESM1.2. *J. Clim.* **32**, 2207–2226 (2019).
30. B. Green, J. Marshall, Coupling of trade winds with ocean circulation damps ITCZ shifts. *J. Clim.* **30**, 4395–4411 (2017).
31. S. M. Kang, Y. Shin, S.-P. Xie, Extratropical forcing and tropical rainfall distribution: Energetics framework and ocean Ekman advection. *NPJ Clim. Atmos. Sci.* **1**, 20172 (2018).
32. C. R. Mechoso *et al.*, Can reducing the incoming energy flux over the Southern Ocean in a CGCM improve its simulation of tropical climate? Southern Ocean-Tropics Link in a CGCM. *Geophys. Res. Lett.* **43**, 11057–11063 (2016).
33. S. M. Kang *et al.*, Extratropical–Tropical Interaction Model Intercomparison Project (Etin-Mip): Protocol and initial results. *Bull. Am. Meteorol. Soc.* **100**, 2589–2606 (2019).
34. S. M. Kang, K. Park, Y. Hwang, W. Hsiao, Contrasting tropical climate response pattern to localized thermal forcing over different ocean basins. *Geophys. Res. Lett.* **45**, 12544–12552 (2018).
35. Y. Shin *et al.*, Evolution of the tropical response to periodic extratropical thermal forcing. *J. Clim.* **34**, 6335–6353 (2021).
36. S.-P. Xie, S. G. H. Philander, A coupled ocean-atmosphere model of relevance to the ITCZ in the Eastern Pacific. *Tellus A Dyn. Meterol. Oceanogr.* **46**, 340–350 (1994).
37. Y.-T. Hwang *et al.*, Relative roles of energy and momentum fluxes in the tropical response to extratropical thermal forcing. *J. Clim.* **34**, 3771–3786 (2021).
38. J. C. H. Chiang, C. M. Bitz, Influence of high latitude ice cover on the marine Intertropical Convergence Zone. *Clim. Dyn.* **25**, 477–496 (2005).
39. S. Bony, Marine boundary layer clouds at the heart of tropical cloud feedback uncertainties in climate models. *Geophys. Res. Lett.* **32**, L20806 (2005).

40. H. Zhang, A. Clement, P. Di Nezio, The South Pacific meridional mode: A mechanism for ENSO-like variability. *J. Clim.* **27**, 769–783 (2014).
41. M. J. Webb, F. H. Lambert, J. M. Gregory, Origins of differences in climate sensitivity, forcing and feedback in climate models. *Clim. Dyn.* **40**, 677–707 (2013).
42. F. Brient, T. Schneider, Constraints on climate sensitivity from space-based measurements of low-cloud reflection. *J. Clim.* **29**, 5821–5835 (2016).
43. T. A. Myers *et al.*, Observational constraints on low cloud feedback reduce uncertainty of climate sensitivity. *Nat. Clim. Chang.* **11**, 501–507 (2021).
44. M. R. England, L. M. Polvani, L. Sun, C. Deser, Tropical climate responses to projected Arctic and Antarctic sea-ice loss. *Nat. Geosci.* **13**, 275–281 (2020).
45. Y. Lin, Y. Hwang, J. Lu, F. Liu, B. E. J. Rose, The dominant contribution of Southern Ocean heat uptake to time-evolving radiative feedback in CESM. *Geophys. Res. Lett.* **48**, e2021GL093302 (2021).
46. Y. Geng *et al.*, CMIP6 intermodel spread in interhemispheric asymmetry of tropical climate response to greenhouse warming: Extratropical ocean effects. *J. Clim.* **35**, 4869–4882 (2022).
47. T. Andrews, J. M. Gregory, M. J. Webb, The dependence of radiative forcing and feedback on evolving patterns of surface temperature change in climate models. *J. Clim.* **28**, 1630–1648 (2015).
48. Y. Dong *et al.*, Intermodel spread in the pattern effect and its contribution to climate sensitivity in CMIP5 and CMIP6 models. *J. Clim.* **33**, 7755–7775 (2020).
49. C. Zhou, M. D. Zelinka, S. A. Klein, Impact of decadal cloud variations on the Earth's energy budget. *Nat. Geosci.* **9**, 871–874 (2016).
50. K. E. Taylor *et al.*, Estimating shortwave radiative forcing and response in climate models. *J. Clim.* **20**, 2530–2543 (2007).
51. H. Kim, A. G. Pendergrass, S. M. Kang, The dependence of mean climate state on shortwave absorption by water vapor. *J. Clim.* **35**, 2189–2207 (2022).
52. M. Yoshimori, J. C. Hargreaves, J. D. Annan, T. Yokohata, A. Abe-Ouchi, Dependency of feedbacks on forcing and climate state in physics parameter ensembles. *J. Clim.* **24**, 6440–6455 (2011).
53. Y.-T. Hwang, D. M. W. Frierson, S. M. Kang, Anthropogenic sulfate aerosol and the southward shift of tropical precipitation in the late 20th century. *Geophys. Res. Lett.* **40**, 2845–2850 (2013).
54. W. R. Frey, E. A. Maroon, A. G. Pendergrass, J. E. Kay, Do Southern Ocean cloud feedbacks matter for 21st century warming? *Geophys. Res. Lett.* **44**, 12447–12456 (2017).
55. M. D. Zelinka *et al.*, Causes of higher climate sensitivity in CMIP6 models. *Geophys. Res. Lett.* **47**, e2019GL085782 (2020).
56. M. J. Webb *et al.*, On the contribution of local feedback mechanisms to the range of climate sensitivity in two GCM ensembles. *Clim. Dyn.* **27**, 17–38 (2006).
57. X. Qu, A. Hall, S. A. Klein, P. M. Caldwell, On the spread of changes in marine low cloud cover in climate model simulations of the 21st century. *Clim. Dyn.* **42**, 2603–2626 (2014).
58. N. G. Loeb *et al.*, Clouds and the Earth's Radiant Energy System (CERES) Energy Balanced and Filled (EBAF) top-of-atmosphere (TOA) Edition-4.0 data product. *J. Clim.* **31**, 895–918 (2018).
59. R. W. Reynolds, N. A. Rayner, T. M. Smith, An improved in situ and satellite SST analysis for climate. *J. Clim.* **15**, 17 (2002).
60. A. H. Young, K. R. Knapp, A. Inamdar, W. Hankins, W. B. Rossow, The International Satellite Cloud Climatology Project H-Series climate data record product. *Earth Syst. Sci. Data* **10**, 583–593 (2018).
61. F. Jia, L. Wu, A study of response of the equatorial pacific SST to doubled-CO2 forcing in the coupled CAM–1.5-layer reduced-gravity ocean model. *J. Phys. Oceanogr.* **43**, 1288–1300 (2013).
62. J. W. Hurrell *et al.*, The Community Earth System Model: A framework for collaborative research. *Bull. Am. Meteorol. Soc.* **94**, 1339–1360 (2013).
63. E. A. Middlemas, J. E. Kay, B. M. Medeiros, E. A. Maroon, Quantifying the influence of cloud radiative feedbacks on Arctic surface warming using cloud locking in an earth system model. *Geophys. Res. Lett.* **47**, e2020GL089207 (2020).
64. E. A. Middlemas, A. C. Clement, B. Medeiros, B. Kirtman, Cloud radiative feedbacks and El Niño–Southern Oscillation. *J. Clim.* **32**, 4661–4680 (2019).
65. K. Sarah et al. ETIN-MIP (Extra-Tropical Interaction Model Intercomparison Project) data. Zenodo. https://zenodo.org/record/3362615. Deposited 9 August 2019.
66. K. Hanjun, K. M. Sarah, K. E. Jennifer & X. Shang-Ping. Subtropical Clouds Key to the Southern Ocean Teleconnections to the Tropical Pacific. Zenodo. https://zenodo.org/record/5792715. Deposited 10 January 2022.